JACS
JOURNAL OF THE AMERICAN CHEMICAL SOCIETY
Communication
pubs.acs.org/JACS

Activatable Fluorescence/MRI Bimodal Platform for Tumor Cell Imaging via MnO_2 Nanosheet–Aptamer Nanoprobe

Zilong Zhao,[†,∥] Huanhuan Fan,[†,∥] Gaofeng Zhou,[‡] Huarong Bai,[†] Hao Liang,[†] Ruowen Wang,[†] Xiaobing Zhang,[†] and Weihong Tan*[,†]

[†]Molecular Science and Biomedicine Laboratory, State Key Laboratory for Chemo/Bio Sensing and Chemometrics, College of Chemistry and Chemical Engineering, College of Biology, and Collaborative Research Center of Molecular Engineering for Theranostics, Hunan University, Changsha 410082, China

[‡]Department of Radiology, First Xiangya Hospital, Central South University, Changsha 410008, China

Supporting Information

ABSTRACT: A novel dual-activatable fluorescence/MRI bimodal platform is designed for tumor cell imaging by using a redoxable manganese dioxide (MnO_2) nanosheet–aptamer nanoprobe. The redoxable MnO_2 nanosheet acts as a DNA nanocarrier, fluorescence quencher, and intracellular glutathione (GSH)-activated MRI contrast agent. In the absence of target cells, neither fluorescence signaling nor MRI contrast of the nanoprobe is activated. In the presence of target cells, the binding of aptamers to their targets weakens the adsorption of aptamers on the MnO_2 nanosheets, causing partial fluorescence recovery, illuminating the target cells, and also facilitating the endocytosis of nanoprobes into target cells. After endocytosis, the reduction of MnO_2 nanosheets by GSH further activates the fluorescence signals and generates large amounts of Mn^{2+} ions suitable for MRI. This platform should facilitate the development of various dual-activatable fluorescence/MRI bimodalities for use in cells or in vivo.

Molecular imaging is a powerful tool for early detection and management of malignant tumors. Synergistic combination of two or more imaging techniques provides solutions able to address multiple issues of sensitivity, resolution, and tissue penetration in tumor diagnosis.[1] For example, magnetic resonance imaging (MRI) has high spatial resolution and tissue penetration but poor sensitivity.[2] While fluorescence signaling has poor tissue penetration, it does have the capacity for subcellular resolution and single-cell sensitivity, in addition to providing fluorescence-guided surgical procedures by videoscope.[3] Thus, a variety of MRI/fluorescence bimodal strategies have been developed for cancer diagnosis and management.[4] However, magnetic resonance and fluorescence signals in these strategies are "always on" regardless of their proximity to, or interaction with, the cancer biomarkers. This results in a poor target-to-background signal ratio, making anatomical features or biological events of interest more difficult to highlight. Development of a targeted bimodality with activatable MRI contrast and fluorescence signals in response to specific biological stimuli would help to maximize the signal from the target and minimize background signal, improving sensitivity and specificity.

MRI contrast agents act by influencing the proton relaxation of the water interacting with, or surrounding, the agents.[5] Activatable MRI strategies have been typically designed using caged complexes to saturate the paramagnetic ions and shield them from water molecules in a coordinated manner. However, because of poor shield efficacy, these activatable contrast agents usually present only modest contrast enhancement under stimuli such as pH,[6] temperature,[7] or presence of metal ions,[8] small molecules,[9] or protein,[10] thus often failing to meet clinical standards, such as only a 54% increase in response to NADH[9c] and a 3-fold enhancement upon a decrease in pH.[6b] Recently, an 11-fold enhancement in T_1-weighted contrast was realized by an activation mechanism based on encapsulated ultrasmall gadolinium oxide nanoparticles in bioresponsive polymer microcapsules capable of triggered release in response to H_2O_2.[11] The micrometer size of the microcapsules limits further application in cancer management. In addition, integrating these activatable contrast agents with an activatable fluorescence signal is challenging.

We report a novel dual-activatable fluorescence/MRI strategy for bimodal cancer imaging using a nanoprobe based on the physisorption of Cy5-labeled aptamers on redoxable MnO_2 nanosheets (Scheme 1). To date, various materials based on Mn, such as $MnCl_2$,[12] manganese chelates,[13] MnO nano-

Scheme 1. Activation Mechanism of the MnO_2 Nanosheet–Aptamer Nanoprobe for Fluorescence/MRI Bimodal Tumor Cell Imaging

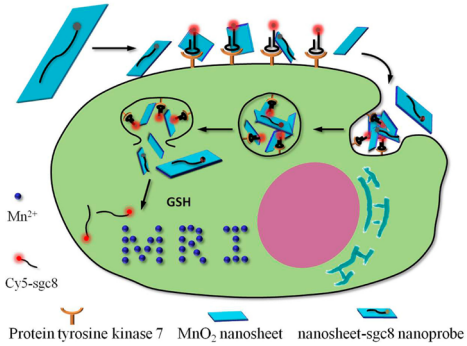

Received: April 2, 2014
Published: July 25, 2014

dx.doi.org/10.1021/ja5029364 | J. Am. Chem. Soc. 2014, 136, 11220–11223

particles,[14] and hybrid nanomaterials,[15] have been used as contrast agents. However, use of redoxable MnO_2 nanosheets as an activatable contrast agent has not been reported. Mn atoms in MnO_2 nanosheets are coordinated in octahedral geometry to six oxygen atoms and shielded from aqueous environment, making no contribution to the protons' longitudinal or transverse relaxation. Thus, the MnO_2 nanosheet is a low T_1- or T_2-weighted contrast agent compared with free Mn^{2+} ions. Also, the MnO_2 nanosheet can efficiently quench fluorescence after fluorophore-labeled aptamers are adsorbed on the MnO_2 nanosheets. Therefore, as the fundamental component of the nanoprobe, the redoxable MnO_2 nanosheet acts as a DNA nanocarrier to deliver target-specific aptamer, fluorescence quencher, and intracellular GSH-activated MRI contrast agent. In the absence of target cells, fluorescence signaling and MRI contrast will not be activated. However, in the presence of target cells, the binding of aptamers to their targets weakens the adsorption of aptamers on the nanosheets, causing partial fluorescence recovery, illuminating the target cells, and facilitating the endocytosis of MnO_2 nanosheets into target cells. Endocytosed MnO_2 nanosheets are then reduced by intracellular GSH to generate large amounts of Mn^{2+} ions for MRI.

MnO_2 nanosheets were prepared by ultrasonicating bulk MnO_2, synthesized by oxidation of $MnCl_2$ by H_2O_2 in the presence of tetramethylammonium hydroxide.[16] As-prepared MnO_2 nanosheets possessed a ζ-potential value of −28.2 mV at 34.8 μg/mL, with their size centered at 141 nm (Figure S1), and had a UV−vis absorption peak centered at 360 nm, with their surface composition identified by X-ray photoelectron spectroscopy (Figure S2). Results from transmission electron microscopy (TEM), selected area electron diffraction analysis, and atomic force microscopy (AFM) indicated that as-prepared MnO_2 presented a polycrystalline sheet structure, with a thickness of about 1.5 nm (Figures 1 and S3).

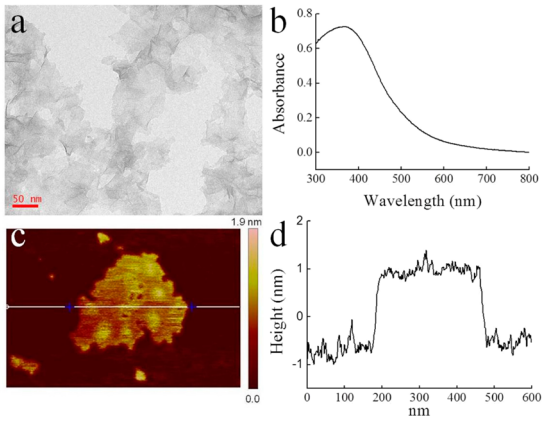

Figure 1. TEM (a), UV−vis absorption spectrum (b), and AFM (c,d) characterization of MnO_2 nanosheets. Black line in (d) represents the height profile of the section in (c) labeled with the white line.

Before preparing the nanosheet-aptamer nanoprobe, we first tested the effect of base number on the physisorption of single-stranded DNA (ssDNA) on MnO_2 nanosheets by fluorescence analysis based on the excellent fluorescence quenching ability of MnO_2 (Figure S4).[17] As shown in Figure 2a, MnO_2 nanosheets exhibited higher quenching efficacy on fluorescein amidate (FAM)-labeled 7-base DNA than equivalent fluorescein, 74% vs 23%. The quenching efficacy increased with the increase of base

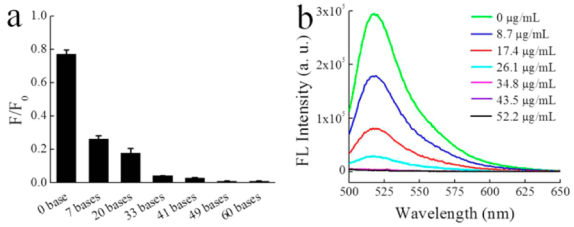

Figure 2. Analysis of adsorption of ssDNA on MnO_2 nanosheets. (a) Adsorption of FAM-labeled ssDNA (100 nM) with different base numbers on MnO_2 nanosheets. F_0 and F are the fluorescence intensities of FAM and equivalent FAM−DNA conjugations before or after mixing with MnO_2 nanosheets, respectively. (b) Adsorption of 60-base DNA (100 nM) on MnO_2 nanosheets at different concentrations.

number and could reach 98% for 60-base ssDNA. Because MnO_2 nanosheets have a negative ζ-potential and no a large electronic conjugate system, the electrostatic interaction and $\pi-\pi$ stacking are excluded for the adsorption of ssDNA on MnO_2 nanosheets. Aromatic fluorescein was identified to weakly adsorb on MnO_2 nanosheets (Figure 2a). In addition, dsDNA had remarkably lower adsorption than ssDNA due to the shielding of nuleobase pairs by the phosphate groups (Figure S5). Thus, the adsorption of ssDNA on MnO_2 nanosheets may be caused by the synergistic physisorption of nucleobases on the basal plane of the MnO_2 nanosheets.[18] The adsorption of a 60-base DNA sequence on MnO_2 nanosheets was very strong and unaffected by 20% fetal bovine serum (FBS) or 1 mg/mL bovine serum albumin (BSA) (Figure S6a). To construct the specific cell-targeting nanosheet−aptamer nanoprobe, aptamer sgc8 (60 bases) targeting protein tyrosine kinase 7 (PTK7)[19] with an extra 19 bases at the 5′-terminus (Table S1) was chosen as a model in this study. The amount of the adsorbed aptamer on 1 μg of as-prepared MnO_2 nanosheets was about 2.9 pmol (Figures 2b and S7).

MnO_2 nanosheets could be dissolved into Mn^{2+} ions in the presence of reductants,[17] such as dithiothreitol (DTT) and GSH. The response of nanosheet−aptamer nanoprobes to different concentrations of DTT was tested by UV−vis and fluorescence spectral analysis. As shown in Figure S6b, the UV−vis absorption band of MnO_2 nanosheets gradually decreased until it disappeared when the concentration of DTT increased from 0 μM to 10 mM, indicating that MnO_2 nanosheets were reduced to Mn^{2+} ions. With the dissolution of quencher, fluorescence of FAM recovered gradually until it was fully recovered (Figures S8 and S9a). However, the nanoprobe showed little chemical or physical response toward other biomolecules, such as some amino acids, BSA, and FBS (Figure S6a), ensuring the stability of the nanosheet−sgc8 nanoprobe before recognizing the target cells. It is worth noting that ∼42% of fluorescence was recovered for Cy5 after treatment with DTT (Figure S9b).

The recognition ability of sgc8 aptamers may be affected by their random physisorption on MnO_2 nanosheets. To determine if the nanoprobe could illuminate the target cells, we examined the fluorescence of PTK7-positive CCRF-CEM cells (human T cell acute lymphoblastic leukemia cell line) and PTK7-negative Ramos cells (human Burkitt's lymphoma cell line) treated with the nanoprobe. CCRF-CEM cells, but not Ramos cells, exhibited a bright red fluorescence signal after mixing with the fluorescence signal-off nanoprobe (Figure

dx.doi.org/10.1021/ja5029364 | J. Am. Chem. Soc. 2014, 136, 11220−11223

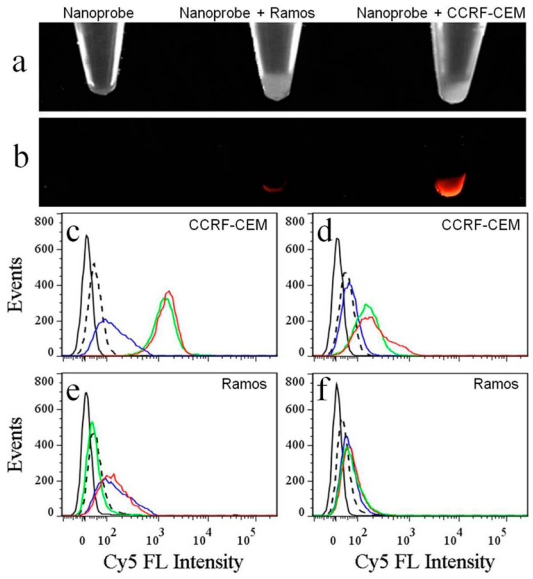

Figure 3. Fluorescence response of MnO_2 nanosheet–sgc8 nanoprobe to target cells. (a) Optical and (b) fluorescent images. (c) Flow cytometric results for the binding and (d) the internalization of the nanoprobe in CCRF-CEM cells. (e) Flow cytometric results of the binding and (f) the internalization of nanoprobe in Ramos cells. Black line represents the autofluorescence of cells. Dashed black line, blue, green, and red lines represent the fluorescence intensity of cells treated with Cy5-labeled library, nanosheet–Cy5-labeled library nanocomplex, Cy5-labeled sgc8 and nanosheet–Cy5-labeled sgc8 nanoprobe.

3a,b). This indicated that the fluorescence response of the nanoprobe was target cell-specific activatable.

Binding and internalization of the nanosheet–sgc8 nanoprobe on target cells were further tested by flow cytometry and confocal laser scanning microscopy (CLSM). As shown in Figure 3c, a higher fluorescence signal was obtained on CCRF-CEM cells treated with nanoprobes (red line) than those treated with nanosheet–library nanocomplexes (blue line) in binding assay. Internalization assay also showed that CEM cells treated with nanoprobes presented a higher fluorescence signal than those treated with nanocomplexes after removing the fluorescent moiety on the cell surface by trypsin (Figure 3d). However, nanoprobes could not recognize PTK7-negative cells and, like nanocomplexes, caused low fluorescence signal on Ramos cells in binding and internalization assays (Figure 3e,f). The selectivity of the nanoprobe was also confirmed by using CLSM (Figures S10 and S11). These results proved that the fluorescence activation of the nanoprobe was specific to target cells. Note that nanoprobes did not enhance the fluorescence signal in binding and internalization analysis when compared with an equivalent sgc8 aptamer (Figure 3c,d).

Based on the variation of adsorption of ssDNA with different base numbers and the dissolution of MnO_2 in the presence of reducing agents, fluorescence activation of nanoprobes on target cells may be attributed to the following two processes: (1) 60-base sgc8 remains adsorbed on MnO_2 after binding to its target protein on the cell surface, due to the extra 19 bases at the 5′-terminus, but binding becomes weakened, causing partial fluorescence activation and facilitating the endocytosis of nanoprobes into target cells. (2) Endocytosed nanocarriers are reduced to Mn^{2+} ions by intracellular GSH, and the adsorbed aptamer is released, leading to fluorescence activation.

To evaluate the effectiveness of the MnO_2 nanosheet as a GSH-activated MRI contrast agent, longitudinal relaxation rate $(1/T_1)$ and transverse relaxation rate $(1/T_2)$ of MnO_2 before and after reduction by GSH were examined. Reduced Mn^{2+} ions exhibited much stronger enhancement in both T_1- and T_2-weighted MRI than the MnO_2 nanosheets (Figure 4).

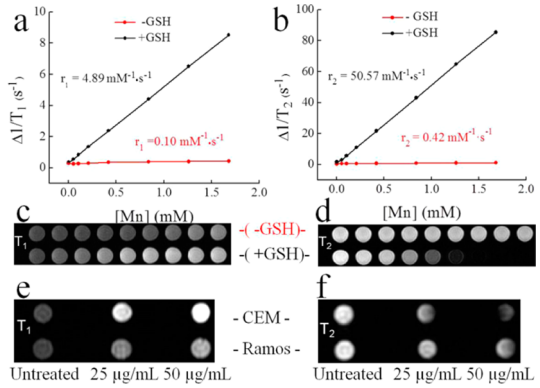

Figure 4. $\Delta 1/T_1$ (a) and $\Delta 1/T_2$ (b) versus Mn concentration for MnO_2 nanosheet solution (red lines) and MnO_2 nanosheet solution treated with GSH (black lines). T_1-weighted (c) and T_2-weighted (d) MRI results obtained from (a) and (b). T_1-weighted (e) and T_2-weighted (f) MRI images of CCRF-CEM cells and Ramos cells incubated with nanosheet–sgc8 nanoprobes at various concentrations in media for 3 h.

Longitudinal relaxivity r_1 and transverse relaxivity r_2, obtained by measuring the relaxation rate as a function of Mn concentration, exhibited 48- and 120-fold enhancement, respectively, when MnO_2 nanosheets were reduced to Mn^{2+} by GSH, which corresponded to the largest enhancement in relaxivity to the best of our knowledge. It was also found that the r_1 and r_2 of the reduced products showed small changes in DPBS and HEPES buffer (Figures S12 and S13). To account for the dramatic enhancements of T_1- and T_2-weighted MRI contrast in our design, consider the following facts: (1) In MnO_2 nanosheets, Mn is shielded from the aqueous environment, decreasing their ability to enhance water proton relaxation; thus, the MnO_2 nanosheet is a kind of weak T_1- and T_2-weighted MRI contrast agent. (2) Once MnO_2 nanosheets are reduced, large amounts of Mn^{2+} ions are generated, and each ion can serve as an MRI contrast agent to enhance the protons' transverse and the longitudinal relaxation times. Therefore, the collective activation of multiple contrast agents generates dramatic enhancements in T_1- and T_2-weighted MRI contrast signals.

The feasibility of a nanosheet–sgc8 nanoprobe for cellular MRI was then evaluated by examination of CCRF-CEM cells and Ramos cells incubated with nanoprobes at different concentrations. CCRF-CEM cells treated with the nanoprobe presented higher T_1- and T_2-weighted MRI contrast than Ramos cells treated with the nanoprobe (Figure 4e,f). The MRI contrast enhancement in target cells may be attributed to the loose adsorption of the 60-base ssDNA on the MnO_2 nanosheets after binding to PTK7, due to the extra bases at the 5′-terminus, facilitating the endocytosis of MnO_2 nanosheets into CCRF-CEM cells. The endocytosed MnO_2 nanosheets are then reduced by intracellular GSH, generating multiple Mn^{2+} ions as MRI contrast agents. The mechanism of intracellular GSH-activated MRI contrast agent was confirmed by experiments showing that, although more MnO_2 nanosheets

dx.doi.org/10.1021/ja5029364 | J. Am. Chem. Soc. 2014, 136, 11220–11223

were kept in the cellular MRI sample of Ramos cells after treatment with 50 μg/mL nanosheet−sgc8 nanoprobe (Figure S14), Ramos cells showed weaker T_1- and T_2-weighted MRI contrast than CCRF-CEM cells. Results indicated that the MRI contrast enhancement was mainly from Mn^{2+} ions and not MnO_2 nanosheets. The contents of Mn in each CEM cell and Ramos cell treated with 25 μg/mL of nanoprobe were determined by inductively coupled plasma optical emission spectroscopy and were 0.078 and 0.032 pg, respectively (Figure S15). Cytotoxicity of MnO_2 nanosheets was also assessed by MTS assay, and results showed that 79% of cells remain alive in the presence of 1 mM of MnO_2 nanosheets (Figure S16).

In summary, we developed a target-cell-activated fluorescence and intracellular GSH-activated MRI contrast agent for bimodal tumor cell imaging via a MnO_2 nanosheet−aptamer nanoprobe. The MnO_2 nanosheet is (1) a nanocarrier to adsorb Cy5-labeled aptamer, (2) a quencher to quench fluorescence, and (3) an intracellular GSH-activated MRI contrast agent. To evaluate the feasibility of a MnO_2 nanosheet−aptamer nanoprobe as an activatable fluorescence/MRI bimodal platform, we have demonstrated its fluorescence activation effectiveness, as well as T_1- and T_2-weighted MRI contrast in situ. We have also demonstrated its potential utility as an activatable fluorescence probe and an activatable MRI contrast agent at the cellular level. Using systematic evolution of ligands by exponential enrichment or in vitro selection, aptamers recognizing different tumor cells have already been selected.[20] We believe that this simple and novel dual-activatable fluorescence/MRI bimodal platform with low background and high sensitivity will have wide applications in cancer cell imaging.

■ ASSOCIATED CONTENT

Supporting Information

Experimental details and additional characterization data. This material is available free of charge via the Internet at http://pubs.acs.org.

■ AUTHOR INFORMATION

Corresponding Author

tan@chem.ufl.edu

Author Contributions

‖Z.Z. and H.F. contributed equally.

Notes

The authors declare no competing financial interest.

■ ACKNOWLEDGMENTS

This work is supported by the National Key Scientific Program of China (2011CB911000), NSFC grants (NSFC 21221003 and NSFC 21327009), and China National Instrumentation Program 2011YQ03012412.

■ REFERENCES

(1) Louie, A. *Chem. Rev.* **2010**, *110*, 3146.

(2) Terreno, E.; Castelli, D. D.; Viale, A.; Aime, S. *Chem. Rev.* **2010**, *110*, 3019.

(3) van Dam, G. M.; Themelis, G.; Crane, L. M.; Harlaar, N. J.; Pleijhuis, R. G.; Kelder, W.; Sarantopoulos, A.; de Jong, J. S.; Arts, H. J.; van der Zee, A. G.; Bart, J.; Low, P. S.; Ntziachristos, V. *Nat. Med.* **2011**, *17*, 1315.

(4) (a) Kim, J. S.; Rieter, W. J.; Taylor, K. M.; An, H.; Lin, W. L.; Lin, W. B. *J. Am. Chem. Soc.* **2007**, *129*, 8962. (b) Janjic, J. M.; Srinivas, M.; Kadayakkara, D. K.; Ahrens, E. T. *J. Am. Chem. Soc.* **2008**, *130*, 2832.

(5) (a) Major, J. L.; Meade, T. J. *Acc. Chem. Res.* **2009**, *42*, 893. (b) Tu, C. Q.; Osborne, E. A.; Louie, A. Y. *Ann. Biomed. Eng.* **2011**, *39*, 1335.

(6) (a) Zhang, S.; Wu, K.; Sherry, A. D. *Angew. Chem., Int. Ed.* **1999**, *38*, 3192. (b) Gianolio, E.; Maciocco, L.; Imperio, D.; Giovenzana, G. B.; Simonelli, F.; Abbas, K.; Bisi, G.; Aime, S. *Chem. Commun.* **2011**, *47*, 1539.

(7) Zhang, S.; Malloy, C. R.; Sherry, A. D. *J. Am. Chem. Soc.* **2005**, *127*, 17572.

(8) (a) Li, W. H.; Fraser, S. E.; Meade, T. J. *J. Am. Chem. Soc.* **1999**, *121*, 1413. (b) Major, J. L.; Parigi, G.; Luchinat, C.; Meade, T. *Proc. Natl. Acad. Sci. U.S.A.* **2007**, *104*, 13881.

(9) (a) Yu, M.; Beyers, R. J.; Gorden, J. D.; Cross, J. N.; Goldsmith, C. R. *Inorg. Chem.* **2012**, *51*, 9153. (b) Aime, S.; Botta, M.; Gianolio, E.; Terreno, E. *Angew. Chem., Int. Ed.* **2000**, *39*, 747. (c) Tu, C. Q.; Nagao, R.; Louie, A. Y. *Angew. Chem., Int. Ed.* **2009**, *48*, 6547.

(10) (a) Nivorozhkin, A. L.; Kolodziej, A. F.; Caravan, P.; Greenfield, M. T.; Lauffer, R. B.; McMurry, T. J. *Angew. Chem., Int. Ed.* **2001**, *40*, 2903. (b) Louie, A. Y.; Hüber, M. M.; Ahrens, E. T.; Rothbächer, U.; Moats, R.; Jacobs, R. E.; Fraser, S. E.; Meade, T. J. *Nat. Biotechnol.* **2000**, *18*, 321. (c) Yang, J. J.; Yang, J.; Wei, L.; Zurkiya, O.; Yang, W.; Li, S.; Zou, J.; Zhou, Y.; Maniccia, A. L.; Mao, H.; Zhao, F.; Malchow, R.; Zhao, S.; Johnson, J.; Hu, X.; Krogstad, E.; Liu, Z. R. *J. Am. Chem. Soc.* **2008**, *130*, 9260. (d) Strauch, R. C.; Mastarone, D. J.; Sukerkar, P. A.; Song, Y.; Ipsaro, J. J.; Meade, T. J. *J. Am. Chem. Soc.* **2011**, *133*, 16346. (e) Yoo, B.; Pagel, M. D. *J. Am. Chem. Soc.* **2006**, *128*, 14032.

(11) Viger, M. L.; Sankaranarayanan, J.; de Gracia Lux, C.; Chan, M.; Almutairi, A. *J. Am. Chem. Soc.* **2013**, *135*, 7847.

(12) Aoki, I.; Takahashi, Y.; Chuang, K. H.; Silva, A. C.; Igarashi, T.; Tanaka, C.; Childs, R. W.; Koretsky, A. P. *NMR Biomed.* **2006**, *19*, 50.

(13) (a) Troughton, J. S.; Greenfield, M. T.; Greenwood, J. M.; Dumas, S.; Wiethoff, A. J.; Wang, J.; Spiller, M.; McMurry, T. J.; Caravan, P. *Inorg. Chem.* **2004**, *43*, 6313. (b) Loving, G. S.; Mukherjee, S.; Caravan, P. *J. Am. Chem. Soc.* **2013**, *135*, 4620.

(14) (a) Na, H. B.; Lee, J. H.; An, K.; Park, Y. I.; Park, M.; Lee, I. S.; Nam, D. H.; Kim, S. T.; Kim, S. H.; Kim, S. W.; Lim, K. H.; Kim, K. S.; Kim, S. O.; Hyeon, T. *Angew. Chem., Int. Ed.* **2007**, *46*, 5397. (b) Kim, T.; Momin, E.; Choi, J.; Yuan, K.; Zaidi, H.; Kim, J.; Park, M.; Lee, N.; McMahon, M. T.; Quinones-Hinojosa, A.; Bulte, J. W.; Hyeon, T.; Gilad, A. A. *J. Am. Chem. Soc.* **2011**, *133*, 2955. (c) Kim, T.; Cho, E. J.; Chae, Y.; Kim, M.; Oh, A.; Jin, J.; Lee, E. S.; Baik, H.; Haam, S.; Suh, J. S.; Huh, Y. M.; Lee, K. *Angew. Chem., Int. Ed.* **2011**, *50*, 10589. (d) Shin, J.; Anisur, R. M.; Ko, M. K.; Im, G. H.; Lee, J. H.; Lee, I. S. *Angew. Chem., Int. Ed.* **2009**, *48*, 321.

(15) Schladt, T. D.; Shukoor, M. I.; Schneider, K.; Tahir, M. N.; Natalio, F.; Ament, I.; Becker, J.; Jochum, F. D.; Weber, S.; Köhler, O.; Theato, P.; Schreiber, L. M.; Sönnichsen, C.; Schröder, H. C.; Müller, W. E.; Tremel, W. *Angew. Chem., Int. Ed.* **2010**, *49*, 3976.

(16) Peng, L. L.; Peng, X.; Liu, B. R.; Wu, C. Z.; Xie, Y.; Yu, G. H. *Nano Lett.* **2013**, *13*, 2151.

(17) Deng, R. R.; Xie, X. J.; Vendrell, M.; Chang, Y. T.; Liu, X. G. *J. Am. Chem. Soc.* **2011**, *133*, 20168.

(18) Zhu, C.; Zeng, Z.; Li, H.; Li, F.; Fan, C.; Zhang, H. *J. Am. Chem. Soc.* **2013**, *135*, 5998.

(19) Shangguan, D. H.; Cao, Z. H.; Meng, L.; Mallikaratchy, P.; Sefah, K.; Wang, H.; Li, Y.; Tan, W. H. *J. Proteome Res.* **2008**, *7*, 2133.

(20) (a) Shangguan, D. H.; Li, Y.; Tang, Z. W.; Cao, Z. C.; Chen, H. W.; Mallikaratchy, P.; Sefah, K.; Yang, C. J.; Tan, W. H. *Proc. Natl. Acad. Sci. U.S.A.* **2006**, *103*, 11838. (b) Daniels, D. A.; Chen, H.; Hicke, B. J.; Swiderek, K. M.; Gold, L. *Proc. Natl. Acad. Sci. U.S.A.* **2003**, *100*, 15416. (c) Chu, T. C.; Marks, J. W.; Lavery, L. A.; Faulkner, S.; Rosenblum, M. G.; Ellington, A. D.; Levy, M. *Cancer Res.* **2006**, *66*, 5989.